ARTICLE NO. 78-1504R

Subsonic VSTOL Aircraft Configurations with Tandem Wings

Julian Wolkovitch*
Vought Corporation, Dallas, Texas

The Prandtl-Munk theory predicts that tandem-wing configurations with large (vertical) gap have substantially lower induced drag than conventional wing-tail configurations of similar span, total lift, and dynamic pressure. Wind-tunnel tests were performed to check the theory for a configuration with equal-span tandem wings with gap/span = 0.25, and a stagger/span = 0.44. The tests show that the tandem-wing induced drag is even lower than theoretically predicted values. The application of tandem wings to VSTOL subsonic aircraft is discussed, and a new type of tandem-wing configuration is described. This employs extreme gull-type dihedral and anhedral on the rear wing. This feature reduces induced drag, and also reduces wetted area by eliminating the need for a separate vertical tail.

Nomenclature

A	= aspect ratio $= b^2/S$
ASW	= antisubmarine warfare
a.c.	= aerodynamic center
b	= span
$\bar{c}$	= mean aerodynamic chord
C_D	= drag coefficient $= D/qS$
$C_{D\,\min.}$	= minimum drag coefficient
C_{D0}	= drag coefficient at zero lift
C_{fe}	= (drag at $C_L = C_{LX}$) $/q \times$ wetted area
C_L	= lift coefficient $= L/qS$
C_{LX}	= lift coefficient at $C_D = C_{D\,\min.}$
C_M	= pitching moment$/qS\bar{c}$
C_n	= yawing moment$/qSb$
C_{n_β}	$= \partial C_n/\partial \beta$
D	= drag
D_i	= induced drag
e	= span-efficiency factor from Eq. (3)
e_x	= modified span-efficiency factor from Eq. (2)
L	= lift
l_T	= horizontal tail moment arm
M_{EXP}	= experimental Munk factor, see Eq. (4)
M_{THEO}	= theoretical Munk factor, see Eq. (5)
N_β	= yaw acceleration per rad β
q	= dynamic pressure
S	= reference area
TOGW	= takeoff gross weight
α	= angle-of-attack
β	= angle-of-sideslip
σ	= Prandtl factor for multiplane induced drag

I. Introduction

CURRENTLY much attention is being given to the design of subsonic VSTOL aircraft for missions requiring long range and endurance. For such missions, certain advantages can be obtained by employing tandem wings of approximately equal span, with the wing tips separated by a large vertical gap. These advantages include: low induced drag, the wide range of possible aerodynamic center locations obtainable through tailoring the chords of the front and rear wings, and the relatively large distances separating the wings from centrally mounted lift/propulsion engines, fans, or propellers. This separation simplifies the airframe structure and improves accessibility.

The initial sections of this paper focus on questions relating to the induced drag of tandem wings. A description is given of tests performed in the Vought 7- ×10-ft low-speed wind tunnel to check the theoretically predicted induced-drag advantage of tandem-wing over conventional wing-tail configurations. The other advantages listed above are discussed in subsequent sections of this paper. Finally, tandem-wing configurations are compared with conventional configurations on the basis of takeoff gross weights of aircraft sized to perform a given mission.

II. Theoretical Induced Drag of Tandem Wings

The induced drag of a general pair of airfoils of spans b_1, b_2, carrying lifts L_1, L_2 is given by Eq. (1).

$$\pi q D_i = \left(\frac{L_1}{b_1}\right)^2 + 2\sigma\left(\frac{L_1}{b_1}\right)\left(\frac{L_2}{b_2}\right) + \left(\frac{L_2}{b_2}\right)^2 \qquad (1)$$

The Prandtl factor σ depends on the Trefftz-plane configuration, i.e., the projection of the airfoils upon a plane normal to the freestream. According to Munk's stagger theorem,[1,2] σ does not depend upon the longitudinal separation (stagger) of the wings. Graphs of σ for undihedralled (parallel) pairs of airfoils are given by Reid[2] and McLaughlin.[3] For airfoils with dihedral or winglets σ may be computed by Trefftz-plane or vortex-lattice programs, e.g., Lamar.[4] (Note that certain vortex-lattice methods, such as that of Ref. 5, are not suitable for this purpose.)

Durand[2] tabulates both the Prandtl factor and also the induced-drag parameters computed from Eq. (1). These Prandtl factors are accurate to within 1%, but as noted by Laitone,[6] there is an unfortunate labeling error in the tables in Ref. 2. The first row heading is incorrectly labeled gap/(mean span) instead of gap/(span of largest span surface).

Equation (1) applies for optimal (e.g., elliptic) span-loading. The case of nonoptimal span-loadings, where the span-efficiency factor for each isolated wing is e_1, e_2, respectively, is discussed by Reid.[1] Reid shows that acceptable accuracy is obtained by replacing b_1^2 in the first term of Eq. (1) by $e_1 b_1^2$, and b_2^2 in the last term by $e_2 b_2^2$, with no change in the middle term.

Equation (1) predicts considerable induced-drag savings for configurations with large gap measured in the Trefftz-plane. To illustrate this, Fig. 1 graphs Eq. (1) for a typical aft-tail configuration, and also for an equal span-tandem or biplane configuration with various ratios of gap to span. As shown in Fig. 1, not only is the minimum induced drag less for the

Presented as Paper 78-1504 at the AIAA Aircraft Systems and Technology Conference, Los Angeles, Calif., Aug. 21-23, 1978; submitted Sept. 11, 1978; revision received Feb. 20, 1979. Copyright © American Institute of Aeronautics and Astronautics, Inc., 1978. All rights reserved. Reprints of this article may be ordered from AIAA Special Publications, 1290 Avenue of the Americas, New York, N. Y. 10019. Order by Article No. at top of page. Member price $2.00 each, nonmember, $3.00 each. **Remittance must accompany order.**

Index categories: Aerodynamics; Configuration Design.

*Senior Staff Engineer.

equal-span configuration, but the excess above the minimum (i.e., the trim drag) is less sensitive to off-optimum division of total lift between the two lifting surfaces.

III. Vought Tandem-Wing Test

The Prandtl-Munk theory underlying Eq. (1) has been verified experimentally for configurations of moderate stagger, but no verification was available for highly staggered configurations, i.e., "tandem wing" rather than "biplane." Therefore, Vought performed a wind-tunnel test on the tandem-wing model shown in Fig. 2.

The model description is as follows:[7,8] The fuselage is mainly fabricated from wood with a metal insert for the sting. A bubble instrument can be mounted within the fuselage so that the model pitch attitude can be verified without dependence on sting-deflection calibrations. The front wing employs a GAW-1 17% thickness/chord airfoil and is fabricated from metal. It is mounted at a fixed incidence of 6.0 deg relative to the fuselage waterline. The waterline is the reference for measurements of angle-of-attack α. A root fillet is built up from wax on a metal baseplate cut to the planform shown in Fig. 2. The rear wing is mounted on top of the vertical tail by means of a tongue so that its incidence can be set at one of several settings. The rear wing is made from wood. Although the same tapes were employed to yield identical planforms and airfoils for the front and rear wings, the surface finish of the rear wing is inferior to that of the front wing, and less smooth than is usual for wind-tunnel models.

To fix transition, #60 grit was applied densely in 1/10-in. wide bands at 5% chord on upper and lower surfaces of both wings and both sides of the vertical tail. A similar transition strip was applied around the fuselage 3-in. aft of the nose. Standard static-tares, base-pressure, and wind-tunnel wall corrections were applied to the measured data. For purposes of selecting the appropriate wall correction, all runs with only a single wing were considered to be "tail-off," and all tandem configurations were considered to be "tail-on." It has been found that the wall corrections and the base-pressure corrections were both small. The tunnel cross-section was 7×10 ft. The test Reynolds number was 0.52×10^6, based on the mean geometric chord of either wing, and the Mach number was 0.17. The model span was 3.56 ft, the reference chord was 0.474 ft, and the reference area was 1.584 ft^2, corresponding to the span, mean aerodynamic chord, and gross area of either wing.

Several problems arise in comparing experimental drag data with the predictions of Eq. (1). Some of these problems occur because the derivation of Eq. (1) assumes that both airfoils are untwisted and have no spanwise variation of camber. As shown by Igoe, Re, and Cassetti,[9] for an isolated airfoil with twist and/or a spanwise variation of camber, the drag polar takes the form:

$$C_D = C_{D\min.} + \frac{(C_L - C_{LX})^2}{\pi A e_X} \tag{2}$$

instead of the classical form:

$$C_D = C_{D_0} + \frac{C_L^2}{\pi A e} \tag{3}$$

The "offset" form of drag polar described by Eq. (2), with $C_{D\,\min.}$ attained at $C_L = C_{LX} = 0$, is predicted to occur for a twisted wing even if viscous drag is negligible and full leading-edge suction is maintained. Viscous effects, discussed below, further offset the drag polar, but this effect is supplementary to the above-mentioned offset due to twist and camber.

The derivation of Eq. (1) assumes that each airfoil of the pair has (when isolated) a nonoffset drag polar of the form of Eq. (3). Therefore, when performing an experimental

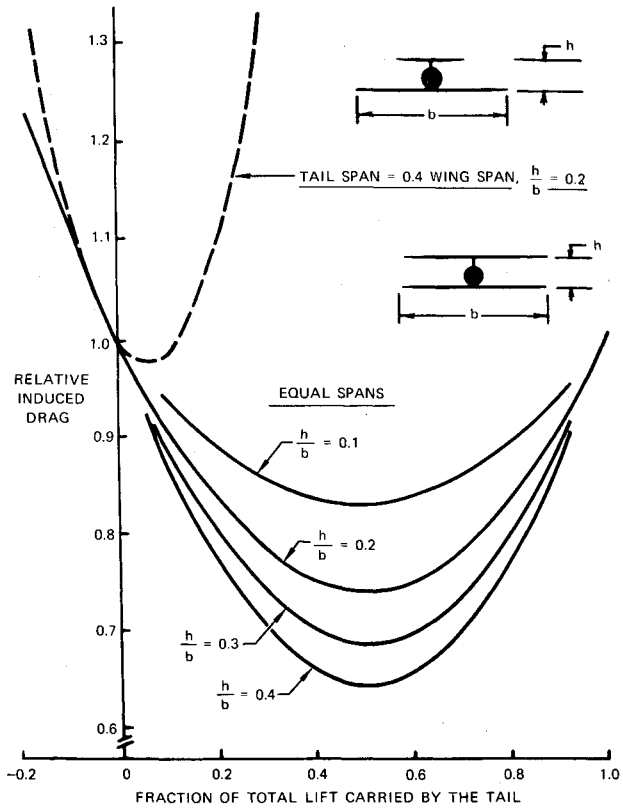

Fig. 1 Induced drag for tandem-wing and conventional wing-tail arrangements with optimal span-loadings.

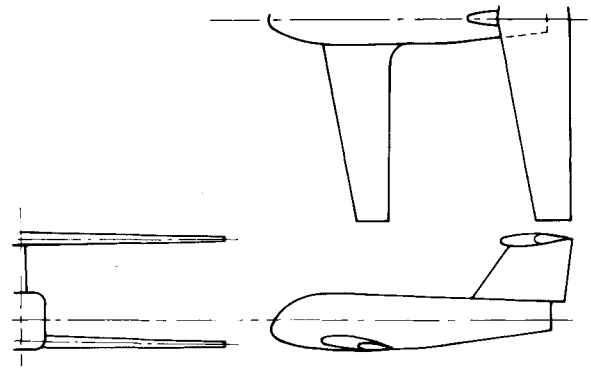

Fig. 2 Vought tandem-wing research model.

verification of Eq. (1) by testing a pair of airfoils, it is desirable that both airfoils should be untwisted and without spanwise variations of camber. The wings of the model shown in Fig. 2 satisfied these conditions, although the masking of the front wing by the fuselage in effect violates these conditions at the center section of the front wing.

Viscous effects cause the airfoil drag coefficient to vary with angle-of-attack even in two-dimensional flow. Such viscous effects are dependent on Reynolds number. A principal goal of the Vought tests was to investigate the validity of Eq. (1) which is derived on the assumption of inviscid flow. Therefore it was desirable that the tests should compare monoplane vs tandem-wing configurations at the same Reynolds number. This was accomplished as follows:

Tests were conducted on three principal configurations: 1) both wings on (BVWFT), 2) rear wing off (BVWF), and 3) front wing off (BVT). "WF" denotes front wing and fillet. The parasite and induced-drag characteristics of configurations BVWF and BVT were not identical. Consequently, the percentage improvement in induced drag

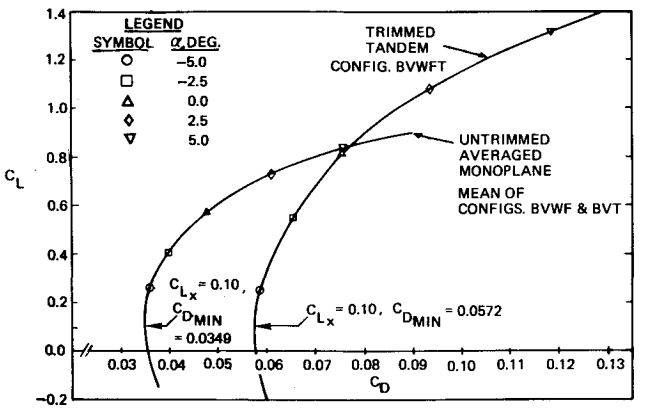

Fig. 3 Comparison of averaged monoplane and tandem-wing drag polars.

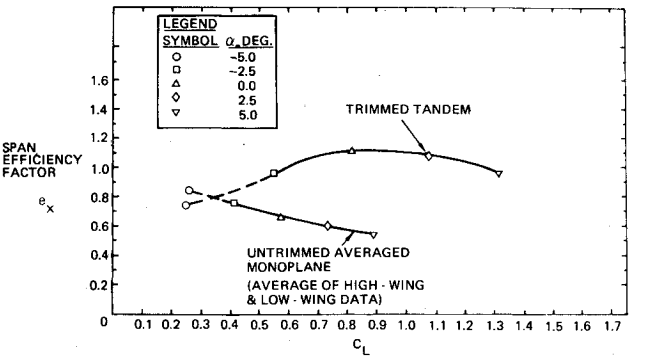

Fig. 4 Comparison of span-efficiency factors: tandem-wing vs monoplane.

provided by the tandem arrangement depends upon whether configuration BVWF or BVT is chosen as the baseline. To obviate any bias due to this choice we take as our baseline a drag polar formed by averaging BVWF and BVT at equal C_L's (for all configurations the same reference area was used). The resulting drag polar is called the drag polar of the "averaged monoplane" designated ½ (BVWF + BVT). The averaged monoplane is untrimmed (since it has only one lifting surface) and has constant incidence angles on the front and rear wings of 6.0 and 6.1 deg, respectively, with no twist on either wing. The tandem configuration BVWFT is trimmed about a point located 35% of the distance between the wing-quarter mean geometric chords, which represents a possible c.g. position. This trim is achieved by varying the rear-wing incidence, leaving the front wing at 6.0 deg throughout.

The averaged monoplane concept described above eliminates Reynolds number as a variable in the comparison of monoplane induced drag vs tandem-wing induced drag. It has the disadvantage that the wing area of the tandem configuration BVWFT is twice that of the averaged monoplane ½ (BVWF + BVT), hence the wetted area and zero lift drag are correspondingly different between BVWFT and ½ (BVWF + BVT). This does not correspond to a comparison between a full-scale tandem-wing configuration and a conventional configuration designed to accomplish the same mission. Such full-scale aircraft would have approximately equal wetted areas. Proper allowance is made for these considerations in the final section of this paper titled Full-Scale Applications. The tandem-wing vs averaged monoplane comparisons presented in the next section of this paper relate principally to verifying the induced drag predicted by Eq. (1).

IV. Test Results

Figure 3 shows the measured drag polars for the untrimmed averaged monoplane and the trimmed tandem configuration. Note that the reference area used to define C_L and C_D is the same for both configurations, although the gross wing area of the tandem is double that of the averaged monoplane.

Although it is clear from Fig. 3 that a substantial reduction in induced drag is provided by the tandem-wing arrangement, it is not a simple matter to compare this reduction with that predicted from Eq. (1). This is because the minimum drag occurs at a nonzero lift coefficient, which we denote as C_{LX}. Hence the classical form of drag polar, [Eq. (3)], gives a poor fit to the measured data near minimum drag and requires extreme variations in e over the C_L range of interest. A much better fit can be obtained from Eq. (2), repeated below.

$$C_D = C_{D\text{min.}} + \frac{(C_L - C_{LX})^2}{\pi A e_X}$$

Figure 4 shows the variation of e_X with C_L for the trimmed tandem and the averaged monoplane configurations. At $C_L \simeq C_{LX}$ the induced drag is small and hard to measure accurately, hence e_X in this region is sensitive to unavoidable limitations on wind-tunnel balance accuracy. However, at higher C_L values the superior e_X of the tandem configuration is apparent.

The equality of C_{LX} for the averaged monoplane, ½ (BVWF + BVT), and for the tandem configuration (BVWFT) found in this test may be coincidental. Other tests, described later, show C_{LX} increasing when going from a monoplane to a tandem-wing configuration. For a given e_X this provides a further reduction in induced drag.

Comparison with Theory

In comparing the induced-drag characteristics of the tandem and the averaged monoplane, allowance should be made for the extra wing area of the tandem. The gross wing area of the tandem is twice that of the monoplane, although the reference area S (used to define C_L, C_D, etc.) is identical. This is significant because it is normal for e_X to decrease as C_L increases above a certain value, due to loss of leading-edge suction, and flow separation. To avoid introducing any bias into the comparison due to such effects, we use as our figure of merit a parameter M_{EXP}, defined below.

$$M_{\text{EXP}} = \frac{e_x \text{ for tandem wing configuration at any specified } C_L}{e_x \text{ for averaged monoplane at } 0.5 \times \text{specified } C_L} \tag{4}$$

M_{EXP}, therefore, compares tandem-wing trimmed induced drag vs monoplane induced drag at the same wing loading, where wing loading is defined as total lift divided by total gross wing area.

M_{EXP} may be compared with the theoretically derived parameter M_{THEO}, known as the Munk factor. This is a factor originally employed for comparisons of biplane vs monoplane induced-drag characteristics.[1,2] It is obtained by successive application of Eq. (1) to the biplane (or tandem) and monoplane configurations that are to be compared, and ratioing the induced drags. Thus, with equal b_1, for both the maximum spans of the biplane and the monoplane, and optimal span loadings.

$$M_{\text{THEO}} = \frac{(L_1 + L_2)^2}{L_1^2 + 2ab_1 L_1 L_2/b_2 + (b_1 L_2/b_2)^2} \tag{5}$$

To compute M_{THEO} we assume that for the trimmed tandem-wing configuration the following condition is satisfied:

$$\frac{\text{Lift on front wing}}{\text{Lift on rear wing}} = \frac{l_R}{l_F} \tag{6}$$

where l_F, l_R are the distances from the c.g. to the 0.25 $\bar{c}$ points of the front and rear wings, respectively. This assumption is equivalent to neglecting the fuselage moments and the pitching moments of each wing about its own quarter-chord.

A further point to be noted in computing M_{THEO} is that the Trefftz-plane gap, z_T, which determines σ, varies with α, according to the relation:

$$z_T = z\cos\alpha - l\sin\alpha$$

where

z = geometric gap (measured at $\alpha = 0$)

l = geometric stagger (measured at $\alpha = 0$)

The computation of M_{EXP}, and comparison with M_{THEO} are given in Table 1.

Table 1 shows that the Prandtl-Munk theory predicts induced-drag levels which are approximately 14% too high in the region of maximum L/D. It is to be expected that the theory will be conservative at moderate and high lift coefficients because it neglects the downward drift of the vortex sheet shed by the front wing, and thus overestimates the downwash that the front wing induces on the rear wing.

No theory has been published for predicting C_{LX} of tandem-wing configurations. The measured C_{LX} values for the major configurations of Fig. 2 are shown in Table 2. The 0.05 increase between C_{LX} for the "body plus front wing" configuration BVWF and the trimmed tandem agrees with unpublished analyses by J. Wolkovitch and R. T. Stancil of Vought. A similar trend is shown by other tandem-wing tests described later. This is important because the combined effects of an increase in C_{LX} and $M_{\text{EXP}}/M_{\text{THEO}} > 1$ yield a substantial further advantage to the tandem-wing configuration over that predicted by the Prandtl-Munk theory.

This summary of the Vought tandem-wing test is focused mainly on the topic of induced drag. Space does not permit a full discussion of other aspects, but the following points should be noted.

Parasite Drag

Analysis of separate component test data[8] shows that the measured $C_{D\,\text{min.}}$ level for the tandem-wing configuration agrees closely with the sum of $C_{D\,\text{min.}}$ for each component, indicating that interference effects on parasite drag are small.

Pitching Moment

The static margin about the specified-moment center varies with C_L in a smooth but nonlinear manner, rising from 0.165 $\bar{c}$ at $C_{L\,\text{TRIM}} = 0.0$ to 0.533 $\bar{c}$ at $C_{L\,\text{TRIM}} = 1.35$. The resulting rear-wing incidence required to trim is shown in Fig. 5. Since trimmed $C_{L\,\text{max.}}$ is approximately 1.4, 4-deg incidence variation trims the configuration over the C_L range of interest. An all-moving rear wing would probably not be employed on a full-scale tandem-wing aircraft; if elevons of span $b/2$ and chord $\bar{c}/4$ were employed on all wings, the elevon deflection range required to trim for $0 \le C_L \le 1.4$ would be approximately 9.8 deg, which is not excessive.

Stall Characteristics

Excellent stall characteristics were observed. At the stall, the tandem-wing configuration BVWFT exhibits a strong pitch-down tendency with little loss of total lift, and buffeting markedly less than that of the monoplane configuration BVWF.

Directional Stability

No adverse C_{n_β} effects were noted either at moderate or high C_L's. The C_{n_β} levels attained are comparable with conventional aircraft.

Table 1 Calculation of Munk factors

C_L, tandem	0.55	0.815	1.078	1.315
α, deg, tandem	−2.5	0.0	2.5	5.0
Gap/span, Trefftz-plane	0.27	0.25	0.23	0.21
M_{THEO}	1.365	1.350	1.330	1.315
e_X, averaged monoplane (at $C_L/2$)	0.84	0.77	0.69	0.638
e_X, tandem (at C_L)	0.959	1.112	1.067	0.957
M_{EXP}	1.14	1.44	1.546	1.50
$M_{\text{EXP}}/M_{\text{THEO}}$	0.835	1.067	1.162	1.14

Table 2 Measured C_{LX} values for major tandem-wing configurations

Configuration	C_{LX}
BVWF	0.05
BVT	0.15
Averaged monoplane	0.10
Trimmed tandem (BVWFT)	0.10

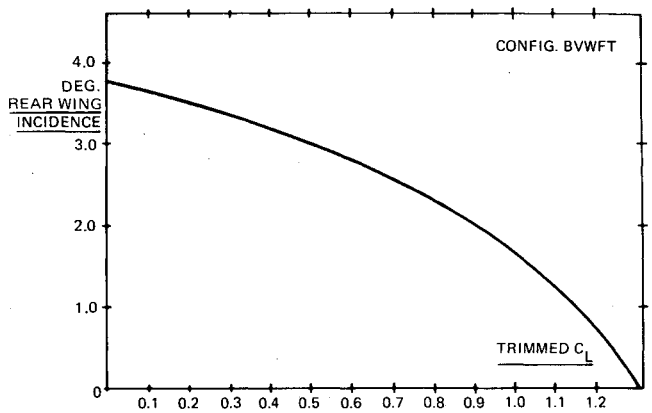

Fig. 5 Rear-wing incidence required to trim; configuration of Fig. 2.

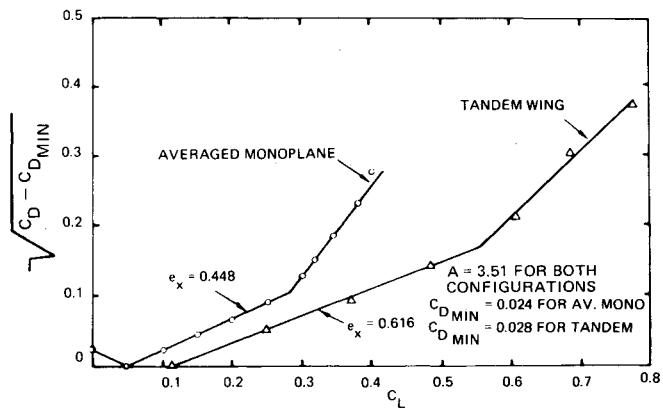

Fig. 6 Induced-drag characteristics for NASA tandem-wing model employing one sweptback and one sweptforward wing.

Other Tandem-Wing Tests

Reference 10 describes tests at a Mach number of 0.3 on a tandem-wing configuration comprised of a sweptback front wing and a sweptforward rear wing. Both wings were of equal span and neither wing had dihedral. The diamond-shaped planform of the wings was symmetric about the aircraft y-axis

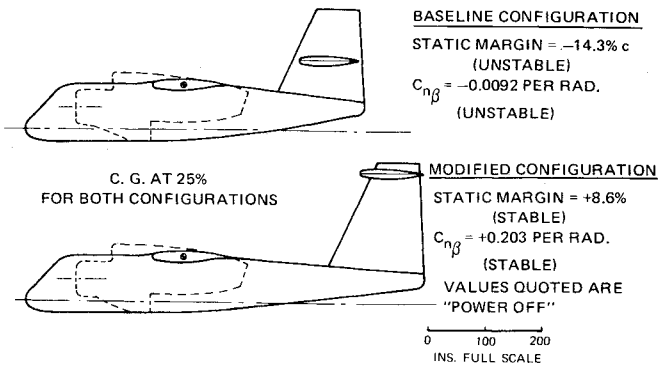

Fig. 7 Comparative configurations.

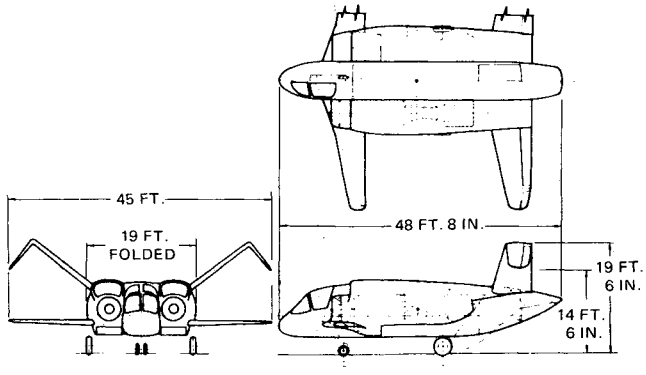

Fig. 8 Vought tandem gull wing.

and the wings were optimally twisted to minimize the induced drag at a design C_L of 0.35. The gross area of both wings combined was used as the reference area, giving an aspect ratio of 3.51 for all configurations. At $\alpha = 0$ the gap/span ratio was 0.178. For some runs the wing tips were connected via endplates, but the endplates were removed for the runs discussed here. Tests were conducted with both wings attached and with each wing removed in turn, so the "averaged monoplane" concept discussed previously can be invoked.

Figure 6 compares the induced-drag characteristics of the averaged monoplane vs the tandem configuration. For the former, Fig. 6 yields $e_X = 0.448$, for the latter, $e_X = 0.616$. Both these values apply below the "breaks" in the graphs of $(C_D - C_{D\,\min.})^{1/2}$ vs C_L. The ratio of the e_X values is 1.37. This is 1.10 times the theoretical Munk factor of 1.24. (The M_{EXP} and M_{THEO} values of 1.37 and 1.24 are both mean values over the C_L range $0 < C_L < 0.285$.) A further saving of induced drag results from the shift of C_{LX} which increases from 0.05 for the averaged monoplane to 0.112 for the tandem-wing configuration.

The low break C_L ($= 0.285$) shown in Fig. 6 is apparently caused by premature stall of the front wing. This is associated with the twist distribution and relatively thin airfoil thickness/chord ratio (6.0%).

In summary, experimental data[7,8,10] show that the induced-drag advantage of certain tandem wings over monoplanes is even greater than predicted by theory.

V. Full-Scale Applications

For subsonic VSTOL aircraft designed for missions involving long range or endurance, the tandem-wing arrangement offers advantages over the conventional aft-tail layout with respect to: 1) induced drag; 2) convenient location of the vertical lift/propulsion system away from the wings; and 3) flexibility in the selection of aerodynamic center location.

The last advantage is explained below by considering a conventional aft-tail layout and showing the performance penalties that it incurs through the additional tail areas required to counter the forward shift of aerodynamic center due to the large nacelles required for VSTOL lift or lift/cruise fans.

Table 3 Comparison of tandem-wing and conventional aircraft for ASW mission (STO)

Characteristic	Tandem wing	Conventional
Takeoff gross weight	42,738	43,725
Span, ft	45.0	58.8
Wing area, ft^2	216.5[a]	450.0
Tail area, ft^2	271.1[b]	107.0
Wetted area, ft^2	2,574.6	2,823.5
C_{fe}	0.00546	0.00536
Cruise L/D	13.2	12.3
Structure weight, lb	10,869	10,917
Propulsion weight, lb	9,003[c]	9,190
Fixed equipment weight, lb	6,598[d]	6,783
Empty weight, lb	(26,470)	(26,890)
Basic useful load, lb	938[e]	944
Mission useful load, lb	4,076	4,076
Fuel, lb	11,254	11,815
Total, lb	42,738	43,725

[a]Front wing. [b]Rear wing projected area. [c]Smaller engine. [d]Smaller control surfaces. [e]Six lb less unusable fuel.

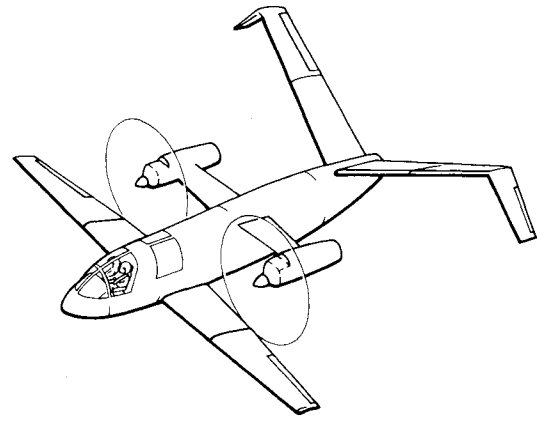

Fig. 9 Turboprop tandem gull wing.

Figure 7 compares two alternative concepts for full-scale configurations. The wing and horizontal-tail geometric characteristics are the same for both configurations. The "short fuselage" configuration of Fig. 7 has horizontal and vertical-tail volume ratios which would be adequate for a CTOL aircraft with smaller nacelles. Wind-tunnel test data indicate that the "short fuselage" is marginally unstable directionally, and also has a negative static margin $= -14.3\%$ $\bar{c}$. These stability characteristics can be improved by adopting a larger vertical tail and by lengthening the fuselage as shown in the lower part of Fig. 7. The resulting effects on performance are of course mission-dependent, but for a representative VSTOL ASW mission the following effects are typical:

Increase of wetted area	= 8.9%
Increase of structure weight	= 8.2%
Increase of fuel weight	= 4.2%
TOGW increase due to added structure	= 2.05%
TOGW increase due to added drag	= 1.15%
Total TOGW increase	= 3.2%

These increases of TOGW include appropriate growth factors.

The levels of static and directional stability noted in Fig. 7 are degraded by power effects. For example, at 150 knots E.A.S. the estimated a.c. shift due to power is 7% $\bar{c}$. Hence for the long fuselage configuration of Fig. 7 the power-on static margin is estimated to be 1.6% $\bar{c}$. Thus the tail-volume ratios for the long fuselage version are not excessively conservative.

The low stability noted above can be ascribed to the large size of the nacelles, their relatively high mass flows, and the forward location of the inlets, which determine the effective moment arm of the inlet-momentum flows. These features are typical of lift/cruise fan VSTOL aircraft, and do not pertain only to the particular configurations shown in Fig. 7. Adequate stability may be obtained through the following alternatives:

1) Larger tail surfaces, as discussed above.
2) Reconfiguring the airframe retaining an aft tail.
3) Control-configured vehicle (CCV) technology.
4) Reconfiguring the airframe to a canard or tandem-wing arrangement.

Although the second and third alternatives must also be given full consideration in any practical design synthesis, the last alternative is the one which we shall discuss in this paper.

Let us now consider some unconventional configurations. The conventional aft-tail layout, with a typical tail area of 25% of the wing area, tends to require the c.g. to be located near the wing quarter-chord. The VTOL lifting units are generally grouped around this c.g. position. This poses some design problems. For example, if the lifting units are closely clustered, they obstruct the wing structure, and pitch-trim moment capability may be small. On the other hand, widely dispersed lifting units (e.g., nose fan plus aft-mounted fans) require lengthy interconnecting shafting, and occupy the fuselage at inconvenient locations, such as ahead of the cockpit. These considerations suggest a canard or tandem-wing layout in which the VTOL lifting units can be grouped around a c.g. which is located between the aerodynamic lifting surfaces. By varying the relative sizes and aspect ratios of two lifting surfaces, the a.c. position required for cruise stability can be set within wide limits, extending almost from one quarter-chord to the other. This allows the nacelle effects on stability to be accommodated. As will be shown, the desired levels of stability can be attained without degrading cruise performance, compared to the short fuselage conventional airplane.

The tandem-wing wind-tunnel model configuration of Fig. 2 is not suitable for scaling up to a full-scale airplane because of potential aeroelastic problems. These arise partly because the rear wing plus vertical tail tends to act like a large T-tail, yielding low antisymmetric stiffness. To avoid this problem we have evolved the configuration shown in Fig. 8. This employs tandem wings of equal spans, the front wing having only slight dihedral, while the rear wing employs extreme dihedral. The objective is to achieve a large gap at the tips, where it is most beneficial for induced drag, while avoiding the structural penalties and folding difficulties of the T-tail. The rear wing tips have sharp negative dihedral and are cambered to act as winglets, giving a further increase in span efficiency. These winglets also provide directional stability. Their effectiveness in this role is enhanced by their location remote from the nacelles. The configuration is stable about all axes, the combined anhedral and dihedral of the rear wing being tailored to yield an overall stable dihedral effect.

A significant advantage of this rear-wing arrangement is that because of its relatively high aspect ratio and its special dihedral, it provides directional stability at the cost of less wetted area than a centrally located vertical tail. The wetted-area penalty of the winglets is offset by their beneficial effect on induced drag.

A vortex-lattice program[4] was applied to this configuration to compute the optimum twist and camber for minimum trimmed induced drag at the cruise C_L. For this configuration, after applying corrections for body effects, at a Mach number of 0.70 the estimated $e_X = 1.66$ at $C_L = 0.6$ (based on total projected area) with $C_{LX} = 0.14$. By contrast, a conventional layout similar to the short fuselage configuration of Fig. 7 (but with winglets) designed to the same specification was estimated to have $e_X = 0.92$ with $C_{LX} = 0.10$ for the same cruise condition.

Vought's ASAP aircraft-design and performance-analysis program was used to optimize the configuration. This program allows such parameters as span, lifting-surface areas, and engine-scale factor to be varied independently to find their optimum values. ASAP models the major structural, aerodynamic, and propulsive effects and all mission constraints. Various missions were studied, comparing the configuration of Fig. 8 vs a conventional aircraft similar to the short fuselage configuration of Fig. 7, but incorporating winglets. The tandem-wing aircraft was designed to have somewhat higher stability than the conventional aircraft. For example, at 115 knots E.A.S. the calculated dimensional-stability derivative N_β for the tandem configuration is 0.375 sec^{-2} greater than the corresponding derivative for the conventional configuration. The tandem-wing airplane is also calculated to have 5.8 in. more maneuver margin than the aft-tail airplane for equal static margins at similar cruise-flight conditions. (This is due to the high pitch damping of the tandem wings.) Both aircraft have equal multimission capabilities. The results presented in Table 3, for an ASW STO mission are typical of all the high-altitude missions studied.

The results shown in Table 3 represent configurations of optimum span giving minimum takeoff gross weights. The much shorter optimum span of the tandem-wing concept indicates that minimum takeoff gross weight is attained by trading off span in order to avoid the weight penalties of high-aspect-ratio lifting surfaces.

The tandem-wing configuration has only 0.91 times the wetted area of the conventional configuration, and has 1.80 times the latter's span efficiency. It is therefore surprising that the weight advantage is only 987 lb, or 2.3%. The explanation is that specific fuel-consumption (SFC) characteristics of the lift/cruise fan powerplants were optimized for the conventional airplane. It was found that the SFC characteristics deteriorated markedly with reduction in cruise thrust. If equal cruise SFC's are maintained for both vehicles, the weight saving is approximately 2500 lb. This highlights a key aspect of the preliminary design process: the propulsion system must be carefully tailored to take advantage of the aerodynamic advantages offered by novel configurations.

The Vought tandem-wing concept shown in Fig. 8 is applicable to other types of propulsion systems. One concept that has been studied is a tilt-propeller configuration shown in Fig. 9. This employs differential collective and cyclic pitch for roll, pitch, and yaw control in hover. Vought's ASAP program was applied to compare this configuration with a similarly powered tilt-wing configuration. For the typical ASW mission the takeoff gross weight of the tandem-wing aircraft was computed to be 92% of the tilt-wing TOGW.

Canard Configurations

The line of demarcation between canard and tandem-wing configurations is somewhat arbitrary and not important here. For present purposes we merely define a canard configuration as one in which the span of the front lifting surface is distinctly less than that of the rear lifting surface. Vought studies of canard configurations indicate that, relative to the above-described tandem-wing configurations, the span-efficiency factor was reduced. Hence the span of the rear wing must be made larger than the span of the tandem wings. It was also found that the combination of this larger span rear wing with winglets was awkward to fold. Because of geometric

folding constraints, the winglet size was limited and a supplementary central fin was required for directional stability. A major constraint on canard design is the $C_{L\,max.}$ of the front surface. Stability can be attained with any ratio of canard/main wing area, but the resulting c.g. position may demand excessively high lift coefficient from the canard for maneuvering flight, and for STOL.

Conclusions

1) The Prandtl-Munk theory predicts substantial savings in induced drag for configurations with wings of approximately equal spans having a large gap between the wings. Wind-tunnel test data show that the measured induced drag of such configurations is less than the theoretically predicted induced drag.

2) Some configurations which exploit the above mentioned induced-drag advantage have cruise performance superior to conventional designs. One example, presented here, employs tandem wings with the rear wing having gull-type dihedral to provide a large gap at the tips, plus winglets which also act as vertical tails.

References

[1]Reid, E. G., *Applied Wing Theory*, McGraw-Hill, New York, 1932.

[2]Durand, W. F., ed., *Aerodynamic Theory*, Vol. II, reprinted by Dover, New York, 1963.

[3]McLaughlin, M. D., "Calculations, and Comparison with an Ideal Minimum of Trimmed Drag for Conventional and Canard Configurations Having Various Levels of Static Stability," NASA TN D-8391, May 1977.

[4]Lamar, J. E., "A Vortex-Lattice Method for the Mean Camber Shapes of Trimmed Noncoplanar Planforms with Minimum Vortex Drag," NASA TN D-8090.

[5]Margason, R. J. and Lamar, J. E., "Vortex-Lattice Fortran Program for Estimating Subsonic Aerodynamic Characteristics of Complex Planforms," NASA TN D-6142.

[6]Laitone, E. V., "Positive Tail Loads for Minimum Induced Drag of Subsonic Aircraft," *Journal of Aircraft*, Vol. 15, Dec. 1978, pp. 837-842.

[7]Vaughan, J. B., "A Low-Speed Wind-Tunnel Test Investigating the Aerodynamic Characteristics of the Vought Tandem-Wing Model in the 7- by 10-Foot Test Section," Rept. 2-53730/7R-3379, Vought Corp., Dallas, Texas, May 1977.

[8]Wolkovitch, J., "Analysis Report of Vought Low-Speed Wind-Tunnel Test of a Tandem-Wing Configuration," Rept. 2-53300/7R-51438, Vought Corp., Dallas, Texas, June 1977.

[9]Igoe, W. B., Re, R. J., and Cassetti, M. D., "Transonic Aerodynamic Characteristics of a Wing-Body Combination Having a 52.5 deg Sweptback Wing of Aspect Ratio 3 with Conical Camber and Designed for a Mach Number of $\sqrt{2}$," NASA TN D-817, May 1961.

[10]Henderson, W. P. and Huffman, J. K., "Aerodynamic Characteristics of a Tandem-Wing Configuration at a Mach Number of 0.30," NASA TM X-72779, Oct. 1975.

From the AIAA Progress in Astronautics and Aeronautics Series

ALTERNATIVE HYDROCARBON FUELS: COMBUSTION AND CHEMICAL KINETICS—v. 62

A Project SQUID Workshop

Edited by Craig T. Bowman, Stanford University and Jørgen Birkeland, Department of Energy

The current generation of internal combustion engines is the result of an extended period of simultaneous evolution of engines and fuels. During this period, the engine designer was relatively free to specify fuel properties to meet engine performance requirements, and the petroleum industry responded by producing fuels with the desired specifications. However, today's rising cost of petroleum, coupled with the realization that petroleum supplies will not be able to meet the long-term demand, has stimulated an interest in alternative liquid fuels, particularly those that can be derived from coal. A wide variety of liquid fuels can be produced from coal, and from other hydrocarbon and carbohydrate sources as well, ranging from methanol to high molecular weight, low volatility oils. This volume is based on a set of original papers delivered at a special workshop called by the Department of Energy and the Department of Defense for the purpose of discussing the problems of switching to fuels producible from such nonpetroleum sources for use in automotive engines, aircraft gas turbines, and stationary power plants. The authors were asked also to indicate how research in the areas of combustion, fuel chemistry, and chemical kinetics can be directed toward achieving a timely transition to such fuels, should it become necessary. Research scientists in those fields, as well as development engineers concerned with engines and power plants, will find this volume a useful up-to-date analysis of the changing fuels picture.

463 pp., 6 × 9 illus., $20.00 Mem., $35.00 List

TO ORDER WRITE: Publications Dept., AIAA, 1290 Avenue of the Americas, New York, N. Y. 10019